Journal of Sustainable Energy & Environment
12 (2021) 45-51

Preparation of RuCo-based catalyst as anode material for redox flow battery by solution route method

A. Thomya* and Y. Khunatron

Department of Mechanical Engineering, Chiang Mai University, Chiang Mai, Thailand
*Corresponding Author: adisorn2@hotmail.com, piakman@gmail.com

Abstract: This research aimed to study the functional groups of active electrocatalysts on the chlorine-side electrode. Catalyst synthesis involved $(Ru_xCo_y)_3O_4$, Co and Ru contents with different Ru/Co molar ratio of 1:9, 2:8, 3:7, 4:6, 5:5. Conditions of catalytic air furnace temperature ranged from 350°C to 500°C. The XRD patterns for catalyst samples confirmed the ruthenium oxide and cobalt oxide phases in the products. The EDS spectra detected ruthenium, cobalt and oxygen in the prepared catalysts. The SEM and TEM images showed more dispersion of catalyst ruthenium oxide on cobalt oxide support surface. Characterization using XRD revealed ~57 nm mean diameter of Co_3O_4 particle sizes, respectively, while TEM technique gave ~85.93 nm mean diameter of $(Ru_{0.1}Co_{0.9})_3O_4$ particle size. The test results of catalyst properties using XRD, SEM, EDS, TEM, SAD techniques showed the same results. HCl was utilized for RFB by spraying the catalyst material in a range of 0.5-1 M on GDL, the chlorine-side, Carbon paper and Carbon cloth. With Carbon paper that had better discharge voltage efficiency, the 0.5 M treatment generated greatest current density and power density. The catalyst material of 0.5 M on Carbon paper achieved the maximum power density of 19.95 $mWcm^{-2}$ and current density of 28 $mAcm^{-2}$ at the voltage efficiency of 69.85%. Hence, the investigation would be beneficial to determine the suitable performance of two-phase flow configuration for redox flow battery with low-cost materials and to gain in-depth understanding of operation characteristics of a redox flow battery using hydrochloric acid as a reactant for new modeling of two-phase flow in cathode.

Keywords: Redox battery, energy storage, hydrochloric acid, catalyst synthesis.

1. Introduction

Redox Flow Battery (RFB) is a potential and efficient energy storage technology which converts and stores electrical energy into chemical energy and releases it in a controlled procedure when required, providing an alternative solution to the problems of balancing power generation and consumption, load levelling and facilitating renewable energy deployment. A typical individual RFB system consists of two external reservoirs which store soluble electroactive electrolytes, two electrodes, a membrane separator and a flow circulation system. The battery generates reduction and oxidation (redox) species between two active materials to store and release energy, respectively. Increasing the concentration of electroactive species and/or the volume of the electrolytes increases the energy storage capacity of a RFB which is a great advantage over other energy storage battery systems [1]. In a H_2/Cl_2 fuel cell, oxygen is substituted by chlorine as the oxidizing agent. Hence, the product from this cell is not water, but more valuable hydrogen chloride. Consequently, the H_2/Cl_2 fuel cell is as much a chemical reactor as an electric generator and the competitiveness of such units is dependent on the prices of both chlorine and HCl [2-3].

Platinum is considered as the best catalyst for hydrogen evolution reaction (HER) with almost zero overpotential and very good durability [4-5]. However, it has important weaknesses due to its high demand, scarcity, and subsequent expensive price, which have led to the necessity of searching for other robust, efficient, and more economic substitutes [6]. Pt-based catalysts are considered to be the most effective catalyst for both electrolyzes and fuel cells. However, their high cost makes it necessary for the development of new and cheaper catalysts that combine platinum with other metals to maintain and even improve catalytic efficiency.

It is also not necessary to use large amounts of precious metals to serve as good electrocatalysts for hydrogen-chlorine regenerative cells. Two of the most widely used electrocatalysts for the chlorine electrode are platinum and ruthenium oxide (RuO_2) [7]. A long-term stability test was performed for the fuel cell with 0.5 $mg_{Pt}cm^{-2}$ Pt on carbon (Pt/C), showing that it was not stable as a cathode material, since Pt dissolved in the presence of chlorine and formed chloroplatinic acid (H_2PtCl_6). Cell performance decreased by 45% using only platinum as a catalyst [8]. Ruthenium oxide (RuO_2) is considered as one of the most active electrocatalyst for chlorine evolution reaction. Using RuO_2 as an electrode material ensures cost reduction, since it is much cheaper than the rest of Pt-group materials. The Ru-Co is found to be a significantly reduced precious metal composition compared with commercial chloride oxidation electrodes [70]. Hydrogen - chlorine regenerative fuel cell that incorporates a $(Ru_{0.09}Co_{0.91})_3O_4$ alloy deposited on carbon as the chlorine electrode with metal loadings of 0.15 $mg_{Ru}cm^{-2}$ and power density of 0.5 Wcm^{-2} results in the cost being negligible when compared to a grid-scale storage system [1].

This research aimed to study the functional groups of active electrocatalysts used for the chlorine-side electrode. Synthesis of catalyst was prepared using $(Ru_xCo_y)_3O_4$, Co and Ru with the Ru/Co molar ratio of 1:9, 2:8, 3:7, 4:6, 5:5. The conditions of catalytic air furnace temperature ranged from 350 - 500°C. The catalysts were physically examined by transmission electron microscopy (TEM), x-ray diffraction (XRD), Scanning Electron Microscope (SEM), Energy-dispersive x-ray spectroscope (EDS) and Selected area diffraction (SAD) to characterize the ring

pattern, particle sizes, and suitable accelerator on Gas Diffusion Layers (GDL), as well as test cell performance [9].

2. Experimental Methods

2.1 Electrode synthesis

The chlorine-side electrode consisted of a Toray carbon paper and ELAT LT2400 carbon cloth incorporated with a single-phase $(Ru_xCo_y)_3O_4$ alloy which was synthesized by standard wet chemical techniques. Before coating, the following protocol was used to clean the carbon paper and carbon cloth: (1) several rinses in DI-H_2O, (2) sonication in DI-H_2O for 10 min, (3) treated with 1 M sulfuric acid at 70°C for 2 hours, (4) dried at 70°C for 1 hour in oven. The substrate is Ruthenium chloride hydrate ($RuCl_3XH_2O$) of Sigma-Aldrich, Cobalt Chloride Hydrate ($CoCl_26H_2O$) of Sigma-Aldrich. The 50 cm^2 clean carbon paper and carbon cloth was then sprayed by mixed suspension of $(Ru_xCo_y)_3O_4$ and 0.15 $mg_{Ru}cm^{-2}$ on GDL. The catalyst material containing a solution of $(Ru_xCo_y)_3O_4$, with Co and Ru contents at the Ru/Co molar ratio of 1:9, 2:8, 3:7, 4:6, 5:5 for $RuCl_3XH_2O$ and $CoCl_26H_2O$ in 12.1 M HCl respectively was dried at 90°C for 20 minutes, and oxidized in an air furnace at 350, 400, 500°C (a 30 min on a ramp followed by a 60 min hold).

The hydrogen-side electrode used 50 cm^2 standard ELAT® gas diffusion electrode (GDE) with a layer of sprayed suspension of mixed 0.05 g carbon black, 10 ml propyl alcohol and 0.21 ml of 11% Nafion solution. Catalyst coated membrane (CCM) was prepared by using the commercial 20% Pt/C for both anode and cathode to produce commercial cell, while using commercial catalysts for hydrogen side was called prepared cell. In preparation process, the catalyst ink was firstly sprayed on a membrane which was placed on a hotplate at 70°C with air as the driving gas. One membrane side had about 50 cm^2 sprayed catalyst area and nearly 0.3 $mg_{pt}cm^{-2}$ for catalyst loading. After one side was finished, the membrane was dried at 70°C for 5 minutes.

The prepared catalyst was physically characterized by x-ray diffraction (XRD, Siemen D500/D501, Cu Kα (λ 1.54), Ni filter, 2θ = 10 – 80º, step 0.02º, step time 1 s), scanning electron microscopy (SEM) equipped with energy dispersive spectroscopy (EDS) (JEOL JSM-5910LV) and transmission electron microscopy (TEM) (JEOL JEM-2010) techniques.

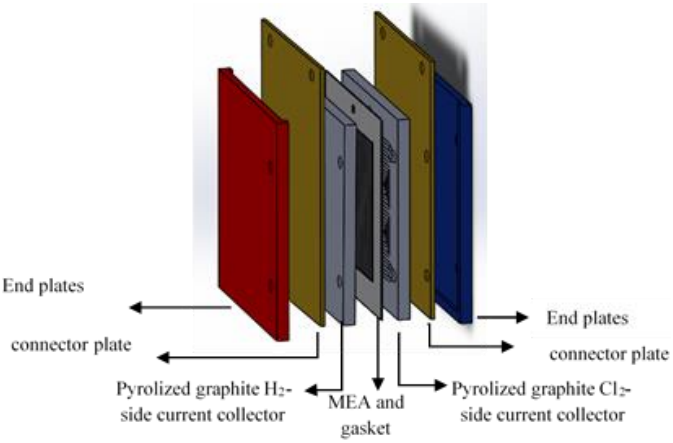

Figure 1. Schematic diagram of a HCl RFB system for concentration and flow rate change experiments in a single cell.

2.2 HCL Redox Flow Battery

Hydrochloric acid (HCl) was electrolyzed to form Cl_2 on the anode side and H_2 on the cathode side of the cell. This process was not spontaneous, so a potential difference must be applied across the electrodes. In discharge mode, H_2 and Cl_2 were fed into the anode and cathode sides of the cell, respectively, to spontaneously form HCl and generate an external current. The proton exchange membrane (typically Nafion) must conduct H^+ ions in both modes (but the direction of conduction switched). If all reactants and products were stored in external tanks, this formed a closed system, resulting in a reversible fuel cell that can function as a flow battery [16].

Table 1. Comparison of recent research on the reversible fuel cell H_2-Cl_2 system function as a flow battery [10].

Electrode		Manufacturing Procedure	Experimental Setup/Operation Conditions		Performance	Reference
Hydrogen side	Chlorine side		Electrolysis	Fuel Cell	Electrolysis	
Pt/C	Pt/C	-	x	j = 40 mA cm^{-2}, T = 50°C 5 – 8 M HCl	EE = 41% and 51%	[11]
Platinized graphite	Percolating porous graphite	-	x	E = 1.0 V	j = 50 mA cm^{-2} PE = 80%	[12]
Platinized graphite	(RuO_2/TiO_2)	flow-through Membrane: Nafion (0.025 cm) SAE: 46 cm^2	H_2 gas; Cl_2 dissolved in HCl j = 100 mA cm^{-2} T = 40 and 80°C Electrolyte = 10% HCl; 8 cm^3 s^{-1}	H_2: non-electrolyte; Cl_2: HCl,j = 100 mA cm^{-2} Cl_2 P = 5 atm, Electrolyte = 10 % HCl	EFE = 85 and 90% (40–80°C)	[13]
Pt-Ir/C 2.5 wt. %Pt; 5 wt. % Ir	Pt-Ir/C 2.5 wt. % Pt; 5 wt. % Ir	Non-membrane SAE: 15 cm^2 Separators:neoprene rubber Electrode distance:6 mm	x	j = 100 mA cm^{-2}, T = 60°C Cl_2 P = 60 mm Hg, Electrolyte = 5 M HCl; 7 mL min^{-1}	MCV = 1.0 V Stable for 300 h	[14]
Pt/C 20 t.%Pt 1 mg_{Pt} cm^{-2}	RuO_2/C 0.8 mg_{Pt} cm^{-2}	Surface area electrode: 6.25 cm^2	x	j = 3 00 mA cm^{-2} T = 25°C Electrolyte = 1 M HCl	MCV = 1.05 V Stable for 120 h	[8]
Pt/C 20 wt. % Pt 0.5 mg_{Pt} cm^{-2}	$(Ru_{0.09}Co_{0.91})_3O_4$ 0.15 mgRu cm^{-2} On GDL	Circular endplates Separators: PTFE, SAE: 2 cm^2 Membrane: Nafion Assembly: Membrane electrode Assembly (MEA)(10.2 nm)	T = 50°C	Anolyte:non-humidified H_2 or humidified H_2(50–100mLmin^{-1}) Catolyte:HCl + bubbles of Cl_2 ,(0 M, 1M, and 2 M) T = 50°C,Cl_2 P = 12–70 psig	Maximum power density = 0.4Wcm^{-2} EFE = 84%	[1]
Pt/C 40 wt. % Pt 0.65 $mg_{Pt}cm^{-2}$	$Ru_{0.3}Ti_{0.6}O_2Pt_{0.1}$/Ti 38 wt. % Ru; 40 wt. % Pt 0.65 mg_{Pt} cm^{-2}	Cell flow-by housing (7.5 cm x 7.5 cm) SAE: 2 cm^2 Membrane: Nafion Assembly: MEA	j = 100 mA cm^{-2} T = 25°C, P = 1 atm Anolyte = 2.0 M NaCl Catholyte = 2.0 M NaCl	E = 0.5 V, T = 25°C, P = 1 atm Anolyte = H_2, microbubbles Catholyte = HClO (1 M HCl + 1 M ClO^-)	H_2 production = 84% EFE = 48%	[15]
Pt/C 20 wt. % Pt 0.3 mg_{Pt} cm^{-2}	$(Ru_{0.1}Co_{0.9})_3O_4$ 0.15 mg_{Ru} cm^{-2} On GDL	Separators: PTFE, SAE: 50 cm^2 Membrane: Nafion 117 GDL:Cabon Paper,Cabon Cloth	Anolyte = H_2 Catholyte = 0.5,1.0M HCl	Anolyte:non-humidified H_2 or humidified H_2(250 mLmin^{-1}) Catolyte: Cl_{2aq}, (0.5 M, 1M) T = 60°C	Maximum power density = 14.5 mWcm^{-2} EFE = 51.47%	This work

The discharge transferred power through a gas flow channel of anode to provide hydrogen to the catalyst.

$$H_2 \underset{\text{charge}}{\overset{\text{Discharge}}{\rightleftharpoons}} 2H^+ + 2e^- \quad E^0 = 0V \qquad (1)$$

Protons (positively charged hydrogen ions) were moving through the membrane combined with proton chlorine. Electrons flew to current collector, then returned to the side of chlorine.

$$Cl_2 + 2e^- \underset{\text{charge}}{\overset{\text{Discharge}}{\rightleftharpoons}} 2Cl^- \quad E^0 = 1.36V \qquad (2)$$

The combination of chlorine, chlorine ions and electrons caused hydrogen ions to combine with chlorine ions, generating HCl and energy across a membrane.

$$H_2 + Cl_2 + 2e^- \underset{\text{charge}}{\overset{\text{Discharge}}{\rightleftharpoons}} 2HCl + electrical\ energy\ E^0 = 1.36V \qquad (3)$$

2.3 Charge/discharge behavior and polarization measurements

RFB prototype in this article, shown in Figs. 1-3. was made of aluminum endplates, brass current collector, graphite flow field with 50 cm^2 reaction area, and Nafion® 117 membranes with catalyst loading conditions under minimums of 0.03 mg/cm^2 Ru on the anode side and mixed Pt of 0.3 mg/cm^2 with 210 µl Nafion on the cathode side coated by ultrasonic spray technique.

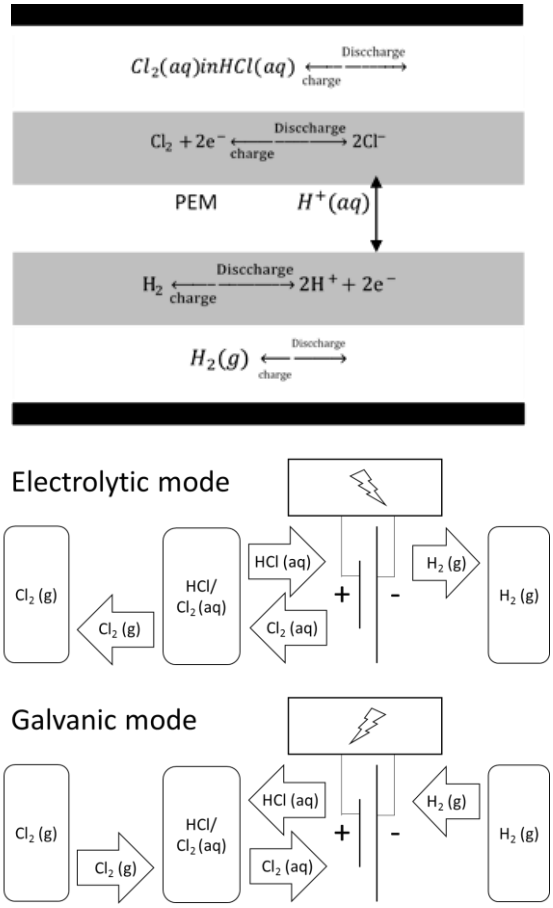

Figure 2. Schematic diagram of a redox flow battery containing hydrochloric acid (HCl RFB) [18].

The endplates were machined from solid aluminum. The 11 cm × 11 cm pyrolytic graphite blocks with single-serpentine flow channels (channel width × dept = 2 mm × 2 mm., landing between channels = 0.4 cm., Fuel Cell Technologies, Inc.) were used as current collectors. Nafion® 117 (0.178 mm thick) was used as a proton-exchange membrane (PEM, Alfa Aesar), and poly-tetrafluoroethylene (PTFE) gasketing was used to seal the cell assembly. Eight bolts (3/8 inch) torqued to 60 lbf·in completed the cell assembly, and PTFE tubing was used to transport reactants and products into and out of the cell. The aluminum endplates were drilled to make holes. All reactant gases (H_2 and Cl_2) were stored inside the fume hood.

This paper aimed to measure the discharging efficiency and the maximum power capacity of redox flow battery that used hydrochloric as electrolyte to meet the demand. The research focused on performance of two-phase flow rate of reactants at the cathode electrode in hydrochloric acid electrolytes.

The concentrations of electrolyte flowing to the RFB prototype were controlled for the range 0.5 to 1 M. Hydrochloric two-phase flow rate of the cathode was in the range of 220 ml/min. The polarization voltage measurement of different concentration levels of electrolyte was conducted and obtained. Then, the efficiency of RFB was calculated from the obtained data during the discharging period [17].

Figure 4 shows that Hydrochloric acid changes color, starting with a clear liquid, then turned yellow and green after being charged and discharged, respectively.

Spraying technique was used to coat a 50 cm^2 cleaned carbon paper and carbon cloth by mixed suspension of 0.15 $mg_{Ru}cm^{-2}$ $(Ru_xCo_y)_3O_4$ on GDL**.**

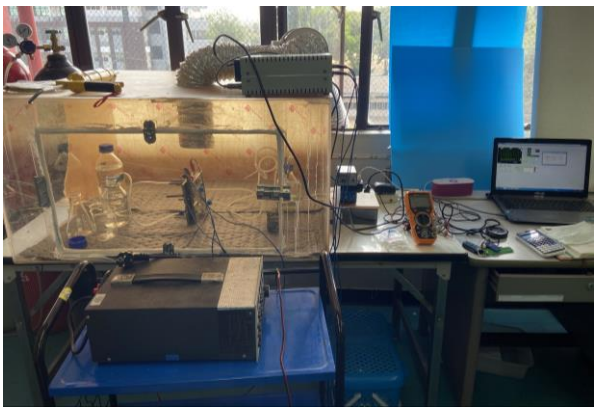

Figure 3. HCl RFB test system utilized in this study.

(a) (b) (c)

Figure 4. The reactant in the cathode electrode. (a) Hydrochloric acid (b) Hydrochloric acid after charged. (c) Hydrochloric acid after discharged.

Figure 5. Spraying technique of catalyst material on GDL.

3. Results and Discussion

Powder XRD patterns of the oxidized $(Ru_xCo_y)_3O_4$, Co and Ru contents with the Ru/Co molar ratios of 1:9, 2:8, 3:7, 4:6, 5:5 in an air furnace at 400°C are presented in Figure 6. The chemical synthesis method used to form the ruthenium-cobalt oxide led to formation of a single-phase alloy that adopted the normal spinel structure of Co_3O_4, with Ru atoms substitutionally replacing Co atoms within this crystal structure. Because the atomic radius of Ru was larger than Co for a given oxidation state and coordination number in a crystal, we would expect the alloy to have a larger lattice constant than that of a pure Co_3O_4 crystal in order to accommodate the larger Ru atoms.[1] The cobalt oxide metal patterns according to JCPDS file no. 78-1969 were also observed along with cobalt oxide peaks at 2θ = 36.84 versus compounds built of Co_3O_4 as show in Table 2, confirming that the feature value of cobalt oxide peak was not equal to 2θ = 36.84, consistent with the above reasoning.

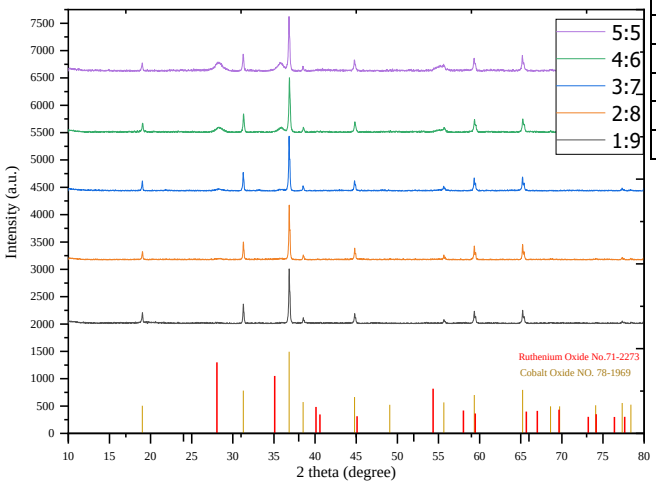

Figure 6. Powder XRD patterns of the oxidized $(Ru_xCo_y)_3O_4$, air furnace at 400°C with the Ru/Co ratios in molarity ranging from 1:9 to 5:5.

Table 2. Compounds built of Cobalt oxide peaks at 2θ.

Ru/Co molar ratios	2θ
1:9	36.87
2:8	36.83
3:7	36.83
4:6	36.88
5:5	36.83

The Ru/Co molar ratios of 1:9, 2:8 and 3:7, however, did not give clear results as they appeared under the broad peak of ruthenium oxide. Peak broadening can be regarded as due to the effects of small size particles. The Ru/Co molar ratios of 4:6 and 5:5 gave visible ruthenium oxide peaks. There was no obvious difference in cobalt oxide peaks of XRD patterns coming from catalysts prepared using the determined Ru/Co molar ratios. However, the appropriate one is 1:9 as increasing molar ratio could form a new element other than RuCo-based catalyst.as show in Figure 6.

To confirm the existence of RuO_2 and Co_3O_4, back-scattered SEM and EDS were performed as shown in Figure 7(a - f) and Table 2. The EDS images showed particle dispersion of the prepared $(Ru_xCo_y)_3O_4$ catalyst and it was found that the Ru atomic percentage increased while the percentage of Co decreased in response to the Ru/Co molar ratios. The numbers of large catalyst particles decreased as the Ru/Co molar ratio increased. The EDS data showed that a higher amount of Ru metal was detected in $(Ru_xCo_y)_3O_4$, Co and Ru contents along with the increase of Ru/Co molar ratio (1:9, 2:8, 3:7, 4:6, 5:5), which was in accordance with XRD peak area measurement.

Figure 7 shows the results of back-scattered SEM of $(Ru_xCo_y)_3O_4$, Co and Ru for the 1:9, 3:7 and 5:5 Ru/Co molar ratios, (oxidized in an air furnace at 400°C) at Magnification X 5000 (Figure 7(a - c) and X 30,000 (Figure 7 (d - f). It was observed from the SEM images that the particle dispersion of $(Ru_xCo_y)_3O_4$ catalyst prepared had higher particle size of cobalt oxide than ruthenium oxide. When increasing the Ru/Co molar ratio, dispersion of Ru particles increased. [9]

Table 3. EDS results of oxidized $(Ru_{0.1}Co_{0.9})_3O_4$ at 400°C in an air furnace.

Ru/Co molar ratios	Element (Atomic %)		
	O	Co	Ru
1:9	52	46.74	0.9
2:8	55.27	40.07	4.66
3:7	57.75	35.52	6.74
4:6	57.77	34.41	7.81
5:5	59.61	29.73	10.66

Figure 8(a) shows TEM image of $(Ru_{0.1}Co_{0.9})_3O_4$ catalyst which illustrates particle agglomeration. The SAD ring pattern, as shown in Figure 7(b), of these particles was indexed to cobalt oxide phases while Ru could not be obtained because of its too small proportion. However, it could be detected in XRD test in a form of Esther spots in the SAD ring pattern which indicated a large particle size. This observation was in accordance with the SEM and XRD results.

Figure 9 shows Powder XRD patterns of $(Ru_{0.1}Co_{0.9})_3O_4$ oxidized in an air furnace at 350, 400 and 500°C. At 350°C, the oxidized catalyst gave a peak corresponding to a hydrate of cobalt chloride, of which the phase was in accordance with JCPDS file no. 00-025-0242 for all patterns at 2θ = 16.12. Cobalt chloride hydrate was the precursor of catalyst synthesis. The remained substrate was oxidized in an air furnace at 350°C, but Cobalt Chloride Hydrate was not found at 400 and 500°C.

Table 4. Comparison of particle sizes from XRD and TEM techniques.

Ru/Co catalyst molar ratio (x:y)	Particle size (nm)	
	XRD Diameter	TEM Diameter
	Co_3O_4	$(Ru_xCo_y)_3O_4$
1:9	53.1	85.93
2:8	55.1	-
3:7	55.0	-
4:6	50.7	-
5:5	72.0	-

Table 4 shows comparison of particle sizes of RuO_2 and Co_3O_4 corresponding to different analytical techniques such as XRD and TEM. It was found that the results of XRD technique had mean particle diameters of ~57 nm for Co_3O_4. It was found that the mean particle diameter of $(Ru_{0.1}Co_{0.9})_3O_4$ investigated by TEM technique was ~85.93 nm.

The study on catalyst properties using XRD, SEM, EDS, TEM and SAD techniques showed that the synthesized catalyst was $(Ru_{0.1}Co_{0.9})_3O_4$ composition with 20% Pt/C commercial catalyst.

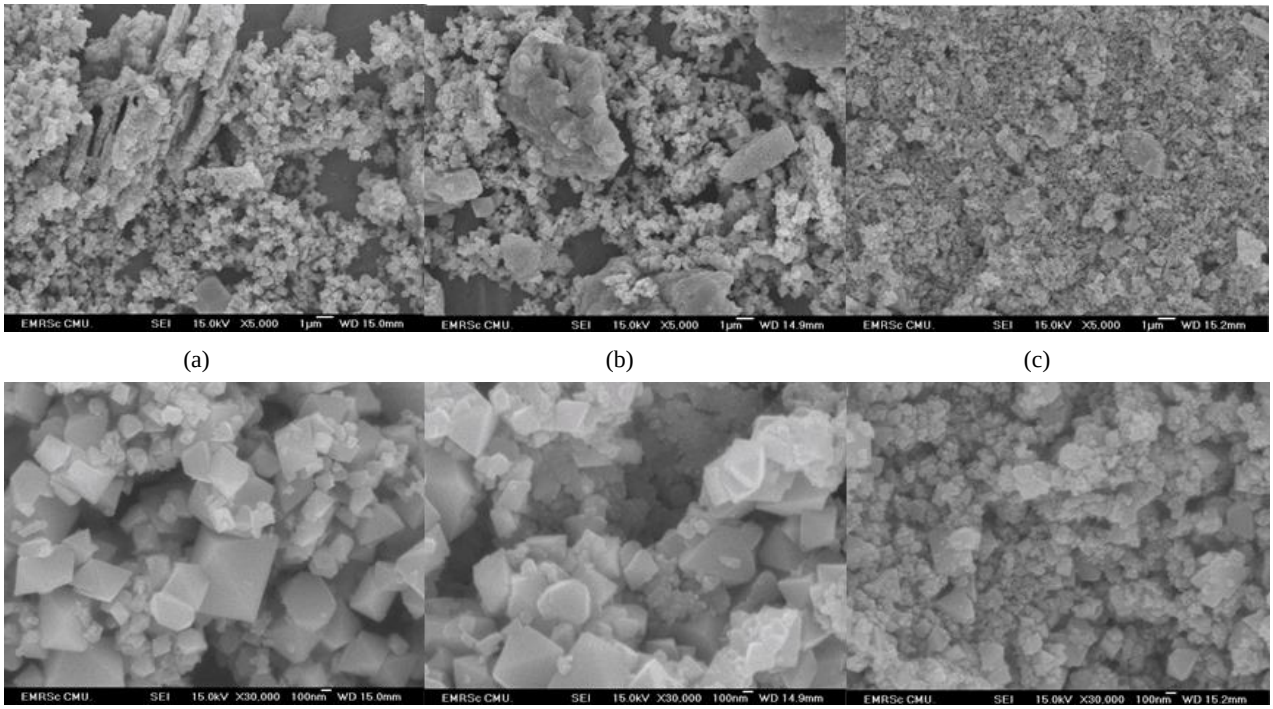

(a) (b) (c)

(d) (e) (f)

Figure 7. Back-scattered SEM of $(Ru_xCo_y)_3O_4$, with the Ru/Co molar ratios of 1:9, 3:7, 5:5, oxidized in an air furnace at 400°C. (a) molar ratio 1:9, magnification X5,000, (b) molar ratio 3:7, magnification X 5,000 (c) molar ratio 5:5, magnification X 5,000, (d) molar ratio 1:9, magnification X 30,000, (e) molar ratio 3:7, magnification X 30,000 (f) molar ratio 5:5, magnification X 30,000.

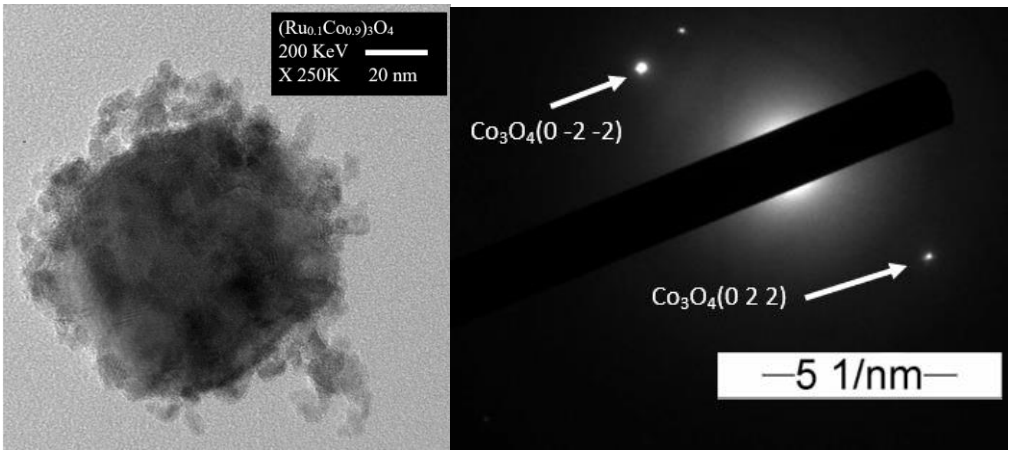

(a) (b)

Figure 8.(a) a TEM image of $(Ru_{0.1}Co_{0.9})_3O_4$ oxidized in an air furnace at 400°C, and (b) SAD ring pattern.

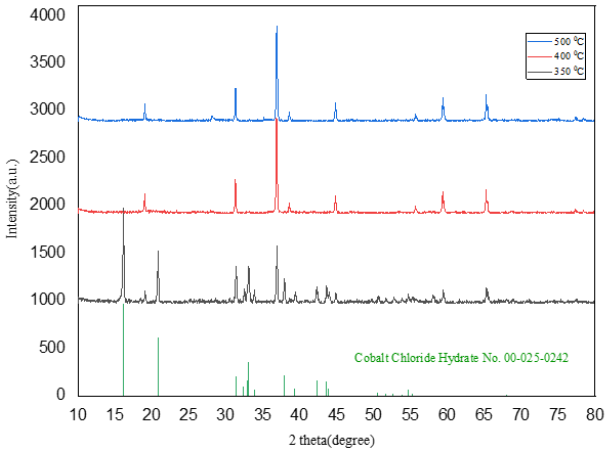

Figure 9. Powder XRD patterns of $(Ru_{0.1}Co_{0.9})_3O_4$ oxidized in an air furnace at 350, 400, 500°C.

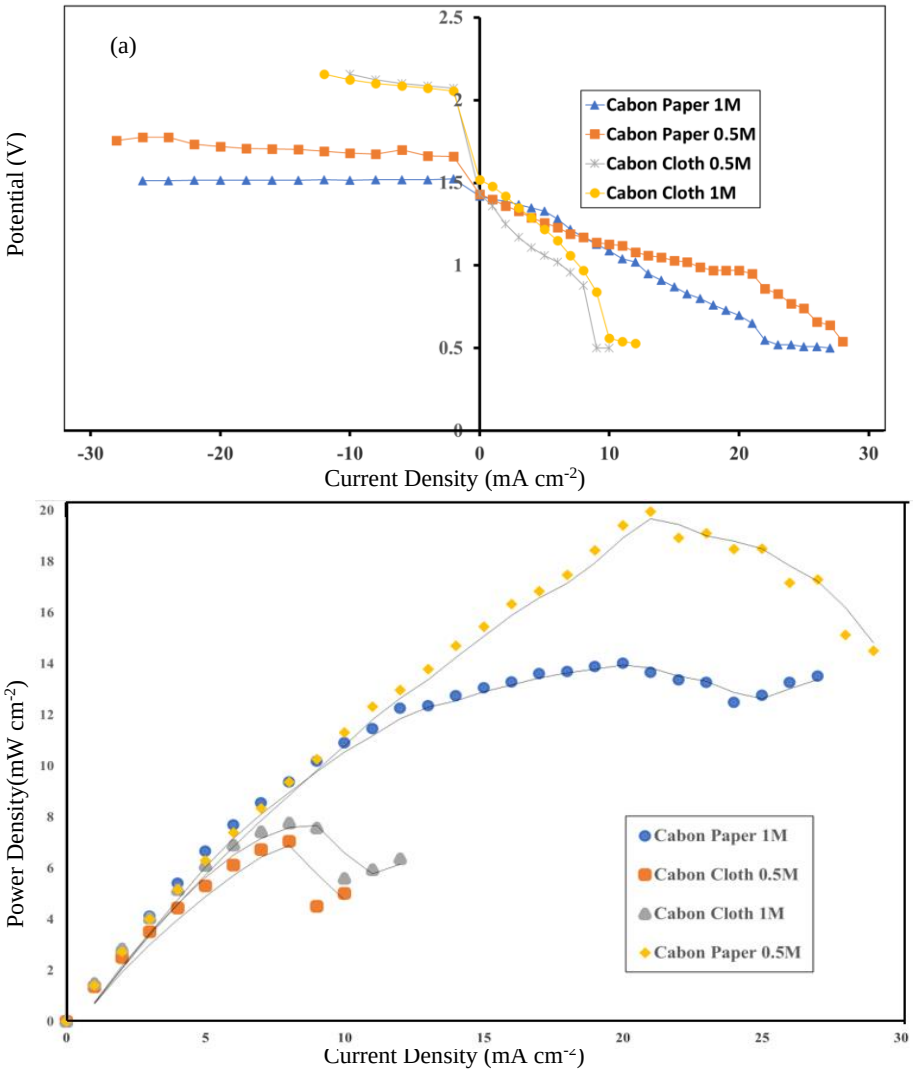

Figure 10. Comparison of catalyst synthesis technique by spraying $(Ru_{0.1}Co_{0.9})_3O_4$ in a range of 0.5 to 1 M on GDL, the chlorine-side, Carbon paper and Carbon cloth. (a) Polarization curve and (b) Power density of discharge process.

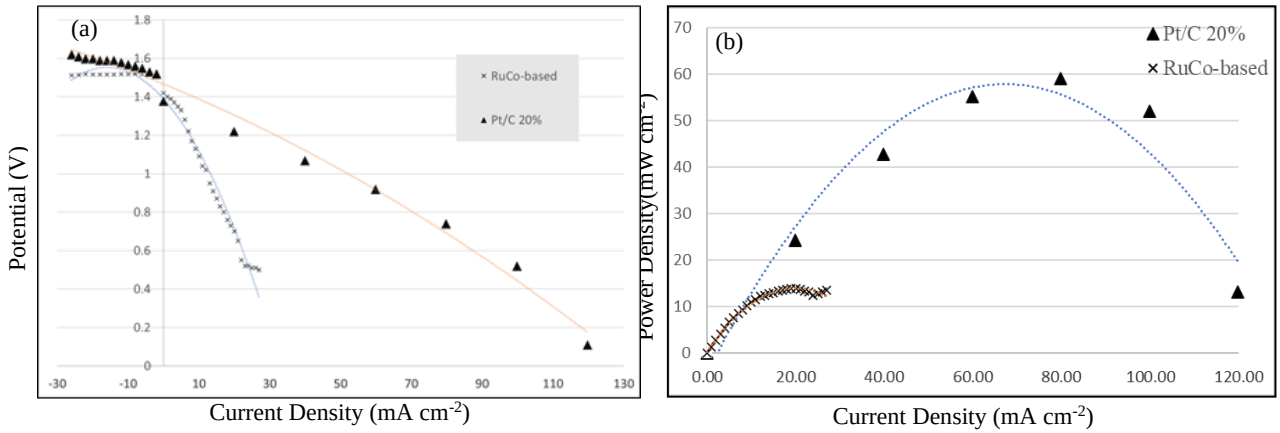

Figure 11. Comparison of $(Ru_{0.1}Co_{0.9})_3O_4$ versus 20% Pt/C with commercial catalyst loading conditions under minimums of 0.03 $mgcm^{-2}$ Ru and 0.5 $mgcm^{-2}$ Pt in 1.0 M HCl RFB. Hydrochloric two-phase flow rate of the cathode was 220 ml/min while the hydrogen-side flow rate of anode was 300 SCCM. (a) Polarization curve (b) Power density of the discharge process.

Form Figure 10, it showed the operations of the cell in HCl RFB, performed by catalyst synthesis technique of spraying the catalyst material on GDL, the chlorine-side, Carbon paper and Carbon cloth, in a range of 0.5 to 1 M, in comparison of the polarization occurred (power density and current density) at the chlorine anode, as well as the discharge voltage efficiency of the cell, Ecell(I)/Eeq in HCl RFB. The polarization curve from the Carbon paper had better discharge voltage efficiency than Carbon cloth, at a concentration of 0.5 M, with the greater current density and power density compared to 1 M.

Carbon paper coated with 0.5 M material had a maximum power density of 19.95 $mWcm^{-2}$ at voltage efficiency

of 69.85% and current density of 28 $mAcm^{-2}$. Carbon paper coated with 1 M material had a maximum power density of 14.5 $mWcm^{-2}$ at voltage efficiency of 51.47% and current density of 27 $mAcm^{-2}$.

Carbon cloth coated with 0.5 M material had a maximum power density of 7.04 $mWcm^{-2}$ at voltage efficiency of 64.71% and current density of 10 $mAcm^{-2}$. Carbon cloth coated with 1 M material had a maximum power density of 7.76 $mWcm^{-2}$ at voltage efficiency of 71.32% and current density of 12 $mAcm^{-2}$.

Form Figure 11, power density, current density and voltage efficiency varied as shown in the comparison of $(Ru_{0.1}Co_{0.9})_3O_4$ versus 20% Pt/C commercial catalyst. The power and current densities were equal to 79.80 $mAcm^{-2}$ and 59.05 $mWcm^{-2}$ at voltage efficiency of 54.41%. $(Ru_{0.1}Co_{0.9})_3O_4$ had a maximum power density of 14 $mWcm^{-2}$ at voltage efficiency of 51.47% and current density of 20 $mAcm^{-2}$. Therefore, it served as a promising way for catalyst synthesis using low-cost materials and to gain in-depth understanding of operational characteristics of redox flow battery using hydrochloric acid as a reactant for a new model of two-phase flow in cathode.

4. Conclusion

Synthesis of $(Ru_xCo_y)_3O_4$ was conducted using different Ru/Co molar ratios to determine Co and Ru contents (x and y). The conditions of the catalytic air furnace temperature ranged from 350 - 500°C. Oxidization occurred in an air furnace at 350°C with the remaining substrate which, was not found at 400 and 500°C. The property examination using XRD, SEM, EDS, TEM and SAD techniques showed that the synthesized catalyst was composition of $(Ru_{0.1}Co_{0.9})_3O_4$ with 20% Pt/C commercial catalyst. Pt/C 20% was a better catalyst, but $(Ru_xCo_y)_3O_4$ was low-cost material.

Cell performances tested with Carbon paper had better discharge voltage efficiency than Carbon cloth. A concentration of 0.5 M gave the greater current density and power density than a concentration of 1 M.

Acknowledgements

The financial support for this research was granted by the Energy Research and Development Institute Nakornping (ERDI), Chiang Mai University, National Research Council of Thailand, and Ministry of Energy of Thailand.

References

[1] Huskinson, B., Rugolo, J., Mondal, S.K. and Aziz, M.J. 2012. A high-power density, high efficiency hydrogen-chlorine regenerative fuel cell with a low precious metal content catalyst, *Energy & Environmental Science*, 5(9), 8690-8698, Available online: http://arxiv.org/abs/1206.2883.

[2] Thomassen, M., Sandnes, E., Børresen, B. and Tunold, R. 2006. Evaluation of concepts for hydrogen – chlorine fuel cells, *Journal of Applied Electrochemistry*, 36(7), 813-819, doi: 10.1007/s10800-006-9140-0.

[3] Fuchs, G., Lunz, B., Leuthold, M. and Sauer, D.U. 2015. Overview of nonelectrochemical storage technologies. In: *Electrochemical Energy Storage for Renewable Sources and Grid Balancing* (pp. 89-102). Elsevier. doi: 10.1016/B978-0-444-62616-5.00007-3.

[4] Du, N., Wang, C., Wang, X., Lin, Y., Jiang, J. and Xiong, Y. 2016. Trimetallic tristar nanostructures: Tuning electronic and surface structures for enhanced electrocatalytic hydrogen evolution, *Advanced Materials*, 28(10), 2077-2084, doi: 10.1002/adma.201504785.

[5] Zhu, L., Lin, H., Li, Y., Liao, F., Lifshitz, Y., Sheng, M., Lee, S.-T. and Shao, M. 2016. A rhodium/silicon co-electrocatalyst design concept to surpass platinum hydrogen evolution activity at high overpotentials, *Nature Communications*, 7, 12272, doi: 10.1038/ncomms12272.

[6] Su, J., Yang, Y., Xia, G., Chen, J., Jiang, P. and Chen, Q. 2017. Ruthenium-cobalt nanoalloys encapsulated in nitrogen-doped graphene as active electrocatalysts for producing hydrogen in alkaline media, *Nature Communications*, 8(1), 14969, doi: 10.1038/ncomms14969.

[7] Jameson, A. and Gyenge, E. 2020. Halogens as positive electrode active species for flow batteries and regenerative fuel cells, *Electrochemical Energy Reviews*, 3(3), 431-465, doi: 10.1007/s41918-020-00067-2.

[8] Thomassen, M., Børresen, B., Hagen, G. and Tunold, R. 2003. H_2/Cl_2 fuel cell for co-generation of electricity and HCl, *Journal of Applied Electrochemistry*, 33, 9-13.

[9] Khonkeng, C., Pantamas, N., Thungprasert, S., Sarakonsri, T. and Chaisena, A. 2013. Preparation of non-noble metals supported on carbon by polymer templation method for solid alkaline fuel cells, *International Journal of Engineering Research and Applications*, 3, 556-559, doi: 10.13140/RG.2.2.12578.04801.

[10] Carvela, M., Raschitor, A., Rodrigo, M.A. and Lobato, J. 2020. Recent progress in catalysts for hydrogen-chlorine regenerative fuel cells, *Catalysts*, 10(11), 1263, doi: 10.3390/catal10111263.

[11] Yoshizawa, S., Hine, F., Takehara, Z. and Kanaya, Y. 1962. Studies of hydrogen-chlorine fuel cell. I. Basic studies of the hydrogen-chlorine fuel cell at low temperature, Journal of The Electrochemical Society of Japan, 30, E10-E16.

[12] Bianchi, G. 1965. Improved porous electrode for studying electrocatalytic reactions of gases and vapors, *Journal of The Electrochemical Society*, 112(2), 233, doi: 10.1149/1.2423503.

[13] Yeo, R.S., McBreen, J., Tseung, A.C.C., Srinivasan, S. and McElroy, J. 1980. An electrochemically regenerative hydrogen-chlorine energy storage system: electrode kinetics and cell performance, *Journal of Applied Electrochemistry*, 10(3), 393-404, doi: 10.1007/BF00617215.

[14] Shibl, S.M.A. and Noel, M. 1993. Platinum-iridium bimetal catalyst-based porous carbon electrodes for H2-Cl2 fuel cells, *International Journal of Hydrogen Energy*, 18(2), 141-147.

[15] Carvela, M., Lobato, J. and Rodrigo, M.A. 2020. Storage of energy using a gas-liquid H_2/Cl_2 fuel cell: A first approach to electrochemically-assisted absorbers, *Chemosphere*, 254, 126795, doi: 10.1016/j.chemosphere.2020.126795.

[16] Chen, J.-Y., Hsieh, C.-L., Hsu, N.-Y., Chou, Y.-S. and Chen, Y.-S. 2014. Determining the limiting current density of vanadium redox flow batteries, *Energies*, 7(9), 5863-5873, doi: 10.3390/en7095863.

[17] Braff, W.A. 2014. *Membraneless Hydrogen Bromine Laminar Flow Battery for Large-Scale Energy Storage*. (p. 163) PhD Thesis, Massachusetts Insitute of Technology.

[18] Thomya, A. and Khunatorn, Y. 2020. Analyzing discharge characteristics of redox flow battery using hydrochloric acid as a reaactant, *2020 International Conference and Utility Exhibition on Energy, Environment and Climate Change (ICUE)*, Pattaya, Thailand, Oct. 2020, pp. 1–7. doi: 10.1109/ICUE49301.2020.9306982.

